AUT Journal of Electrical Engineering
10.22060/EEJ.2024.23038.5584

A novel modeling method for forward-flyback converter and investigating proper design with guidelines to eliminate right half plane zeros

Sayed Mohsen Ahmadi[1], Navid Reza Abjadi[2*], Sayed Vahid Mirmoghtadaei[3] and Ehsan Adib[4]

[1] PhD Student, Faculty of Engineering, Shahrekord University, Shahrekord, Iran

[2] Associate Prof., Faculty of Engineering, Shahrekord University, Shahrekord, Iran

[3] Assistant Prof., Faculty of Engineering, Shahrekord University, Shahrekord, Iran

[4] Prof., Department of Electrical and Computer Engineering, Isfahan University of Technology, Isfahan, Iran

Abstract:

The main advantages of the flyback converter are the simple topology and the isolation of the output from the primary, which is useful for cases where a compact design is required. The converter exhibits inherently nonlinear dynamic behavior, it is also a non-minimum phase system with a zero in the right half plane. In this paper, a combined topology of the flyback converter and conventional forward converter or so-called "forward-flyback converter" is investigated. In addition to the fact that the forward-flyback converter has the inherent advantages of the flyback converter (isolation and simple topology), it is shown that this converter will have better dynamic behavior than the flyback converter. Obtaining the transfer function of the forward-flyback converter through the average state space equations is a difficult task. In this paper, the transfer function of this converter is obtained through a new and simple innovative method. The design of the converter to achieve minimum phase dynamics is also presented. To confirm the analysis performed, laboratory setup of the flyback and forward-flyback converters with a 50-watt power and voltage conversion of 150 to 24 volts DC is implemented, and the obtained results from the measurements show the superiority of the dynamic behavior of the forward-flyback converter compared to the conventional flyback. This work also presents two feedback control designs for the forward-flyback converter using obtained equivalent circuits and models.

Keywords:

Forward-Flyback Converter, Minimum Phase System, Average Model, Transfer Function, Nonlinear Control

∗ Corresponding author's e-mail: abjadi.navidreza@sku.ac.ir

Uncorrected Proof

1. Introduction

One of the most widely used switching converters for powering light loads is the flyback converter. Also, this converter is one of the most widely used switching power supply topologies, which is used in cases such as chargers, computer power supplies, and audio-visual devices. The main advantages of this type of converter are: the possibility of natural isolation of the input from the output, the possibility of implementing multiple outputs on the converter by performing a simple modification on the converter transformer and its simple topology. Normally, the continuous conduction mode of this converter is used more for feeding loads up to 100W loads [1].

One of the important issues in using switching power converters is their dynamic response. To improve the dynamic response of the flyback converter, several researches are done. To analyze and study the dynamic response behavior of switching converters, one of the most efficient methods is the average modeling method [1]. A small signal model of a PWM flyback converter in continuous conduction mode (CCM) considering the effect of parasitic components is given in [2]. In [3], the small-signal analysis of the second-order flyback model has been performed using the state space average model.

In general, average models can be classified based on the resulting system of equations (reduced order to full order) or based on the extraction method (modeling with sampling data, circuit averaging, and state space averaging) [3].

In conventional reduced-order models, the discontinuous variable is considered as a dependent variable and its dynamics are removed from the state equations. Removing the discontinuous variable is undesirable for applications where this variable is used for control purposes [3].

The methods of obtaining the average model of DC-DC PWM converters in discontinuous control mode (DCM) are given in [4-8]. In [9] and [10], a new digital control method is used to improve the dynamic performance of the flyback converter. To improve the efficiency at light loads, the multi-mode control method is used to reduce the frequency when the load is lightened [11-13].

In [14], the control of the flyback converter in current mode with an optically isolated feedback path is presented to achieve complete electrical isolation of the input from the output and to simplify the dynamic behavior of the converter power stage. The performance of the flyback converter in the continuous conduction mode has several advantages, including higher power density, less voltage and current stress, and less electromagnetic interference, but compared to the DCM, the control problem is more difficult, therefore, in [15] a design method for the two-step controller is used in the continuous control mode.

10.22060/EEJ.2024.23038.5584

The peak current mode control method is widely used in DC converters due to its fast response, overcurrent protection, and the possibility of parallel operation. Therefore in [16] a systematic block diagram for the flyback converter controlled by the peak current mode is used to evaluate the dynamic details in high switching frequencies. The transient response of conventional PWM-controlled converters is not fast, but it can be improved if the switching frequency is increased. However, increasing the switching frequency will lead to the adverse effect of switching losses. Also, hysteresis control inherently has characteristics of fast transient response; however, the switching frequency changes dynamically concerning the load conditions, which causes problems for efficiency optimization and the issue of electromagnetic compatibility [17].

Pseudo-resonance control is one of the most common methods to reduce switching power losses in light loads. This method is used in [18]. In this method, the converter mode is automatically changed to the continuous conduction mode to reduce the switching frequency and power losses, especially in light loads. In many applications, the LC filter is used at the output to reduce ripple and switching noise, but the addition of the filter worsens the phase characteristics of the control input to output transfer function and remains zero on the right half plane (RHP) [19].

Some designs of DC-DC converters have RHP zeros in the control input to output transfer function, which slows down the dynamic response of the converter and complicates the control design [20, 21]. The flyback converter also inherently has a RHP zero in the control input to output transfer function, which slows down the response and creates the effect of undershooting or overshooting the output waveform. In fact, in terms of dynamic behavior, such systems are non-minimum phase. The strategies used to eliminate RHP zero of the converter are either based on designing a suitable compensator or based on modifying the circuit topology.

One of the proposed methods to reduce the RHP zero effect for the flyback converter is the operation of the converter in discontinuous mode. In this method, the zero on RHP is shifted towards the switching frequency. Using this method, it is possible to achieve good dynamic performance by designing the control loop, but the current stress in the switch increases and leads to a decrease in efficiency [22]. In [23], the use of leading edge modulation is proposed to convert the flyback converter into a minimum phase system.

In [24], a modified topology is used to eliminate the RHP zero effect in a flyback converter. In [25], an optimized sliding mode current controller is used for power converters with non-minimum phase properties. In [26], a magnetic coupling is used to create a direct path for energy transfer to the output, which caused eliminating the RHP zero effect. In [27], bond graphs are used to retain the system structure and connection between dynamic models and

Uncorrected Proof

transfer functions of control systems, and a comprehensive and general purpose analysis method is presented to remove zeros on RHP. In [28], using classical compensators, two feedback compensation designs are presented for boost and flyback converters to reduce the effect of RHP zero; however, the designs are sensitive to input voltage ripples. In [29], using a magnetic coupling, the RHP zero of the boost converter is omitted which needs an additional coil. In [30], a two loop nonlinear sliding mode control alleviates the RHP zero of the Z-source converter which needs the measurement of current.

In this paper, a forward-flyback converter is investigated. The most important features of the forward-flyback converter are its simple structure, the use of one switch, and high reliability [31, 32]. Also, in comparison with the flyback converter, this converter has a higher power transmission capability. In addition, there is energy transmission in both the on and off states of the switch through the transformer. In other words, the transformer works in both directions of its magnetic curve and this improves the use of the transformer core. This converter has two operation modes: CCM and DCM. In DCM, the stored energy in magnetizing inductor is discharged completely and its current becomes zero. This paper focuses on CCM. In [33], the forward-flyback converter is introduced as a new combination that has only two coils in comparison with the forward converter. In this reference, an additional inductor is used at the output of the converter to connect this converter to the battery and simple control is used to control the output voltage. In [34], a hybrid control method is suggested for the forward-flyback converter with 10 operation modes which is complicated in practical implementation. The converter used in [34] was first proposed in [35]. In [35], the steady-state analysis of the converter and circuit design to ensure zero voltage switching (ZVS) are presented. The same topology is used in [36] with voltage multipliers and soft switching of the converter in DCM is investigated.

Because of the following issues, this paper concentrates on CCM operation:

1. In CCM converters the reduced peak value of current through power switch is an advantage in relation to the DCM converter processing the same power.

2. Because DCM charges and discharges the magnetization inductor completely, the primary current ripple is logically much greater than in CCM. This current variation generates a variating signal, which is then propagated due to the antenna-like behavior of the different components in the primary current loop, generating significant levels of electromagnetic interference (EMI).

3. Regarding regulation and stability of the system, a converter in DCM is easier to compensate than a converter in CCM. This is because the problematic RHP zero appears and introduces instability at lower frequencies when the

converter operates in CCM. DCM pushes the RHP zero to higher frequencies, making the loop easier to be compensated, and therefore offering faster transient response than CCM. Therefore, most of the topics and designed presented in the paper are not required for DCM converter.

In this paper, the dynamical model of the forward-flyback converter of [35] is obtained by a new method. Using this new method, the difficult task of obtaining the full order average model of the converter which has singularity considering the leakage inductance of the transformer, is eliminated. Its transfer function is obtained and the effect of the RHP zero on the dynamic performance of this converter is investigated. It will be shown that, unlike the flyback converter whose structure in the CCM has inherently RHP zero, the structure of this converter in CCM, despite being close to the structure of the flyback converter, can be minimum phase in some performance regions. Also, a comprehensive design is provided to achieve a converter without zero on the RHP. Two applications of the obtained equivalent circuits and models, a type III controller and a feedback linearization nonlinear controller are developed for forward-flyback converter. Finally, some practical results are obtained and presented to validate the proposed model of the converter. The contributions of the paper are highlighted as follows: 1) A novel modeling of forward-flyback converter is proposed in CCM suitable for its analysis and the circuit/control design 2) An analysis of the converter presented to investigate the minimum-phase behavior of the converter 3) A transformer design is presented that leads to minimum-phase behavior 4) The validation of the proposed modeling is performed through three method: AC frequency response, using the model in design a linear controller and using the model in design a nonlinear controller.

2. Forward–Flyback converter

The topology of the forward-flyback converter is shown in Fig. 1. In the new modeling method; the topology of this converter is considered based on the combination of forward and flyback topologies. The function of this converter can be explained based on the two states of switch S1 being on and off.

Uncorrected Proof

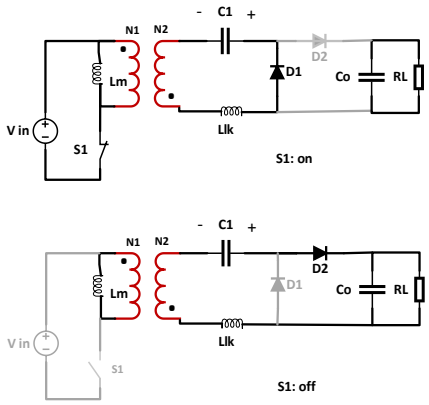

Fig. 1. Equivalent circuit of forward-flyback converter in switch on and off states

When the switch s1 is turned on, the input DC voltage is applied to the primary side of the transformer, and at the same time as the diode D1 is turned on, the capacitor C1 is also charged. In this period, diode D2 is off. When the switch s1 is turned off, the direction of current in the secondary is reversed due to the magnetizing current of the transformer, and diode D1 turns off and diode D2 turns on. In this situation, the voltage of the capacitor C1 and the flyback voltage of the transformer are placed at both ends of the load.

In the flyback converter, when the switch is on, it is not possible to transfer energy to the secondary due to the diode turning off. In fact, the flyback converter transformer works only in one direction of the B-H characteristic curve, so it must be designed in such a way that saturation does not occur. In the flyback converter, there are two operation modes in the switch off state. The first mode corresponds to the mode in which all the energy stored in the magnetizing inductance of the transformer is completely transferred to the secondary before the switch is turned on (discontinuous conduction mode). In the second mode, part of the energy stored in the magnetizing inductance is transferred to the secondary (continuous conduction mode).

The transfer function of the flyback converter in the full energy transfer mode inherently has a RHP zero, but in the non-full energy transfer mode there is no RHP zero.

Considering that the state variables in the forward-flyback converter are dependent on the switch off state and the method of extracting the average model for this converter is complicated, therefore, in the fourth part of this paper, an innovative method to determine the control input to output transfer function of the forward-flyback converter is suggested.

10.22060/EEJ.2024.23038.5584

It is suggested that the converter is divided into two sections, forward and flyback, and the transfer function of each section is calculated, finally, the total transfer function is obtained from them, which represents the equivalent transfer function of the forward-flyback converter.

In the fourth section, the results of modeling and computer simulation of flyback and forward-flyback converters are presented considering the zero effect on RHP.

In the fifth section, the practical results of the implementation of the forward-flyback converter and the comparison of the dynamic behavior of this converter with the conventional flyback converter are presented.

2-1- Dynamics of forward-flyback converter

The description of the dynamics of the forward-flyback converter is based on the determination of the control input to output transfer function using the average model. To obtain the average model, the state variables of the forward-flyback converter including the current of the magnetizing transformer, capacitor voltage C1 and output capacitor voltage Co are considered. However, because the state variables depend on each other in the off state, the calculation of the average model will be complicated. Therefore, to determine the control input to output transfer function of the converter, a new and innovative method has been used in this paper.

In this method, the converter topology is separated into two sections, forward and flyback sections, and the transfer function of each section is calculated separately, and then the total transfer function is calculated. Fig. 2 illustrates how the converter works and how the voltages of the capacitors are generated in the on and off states of the switch.

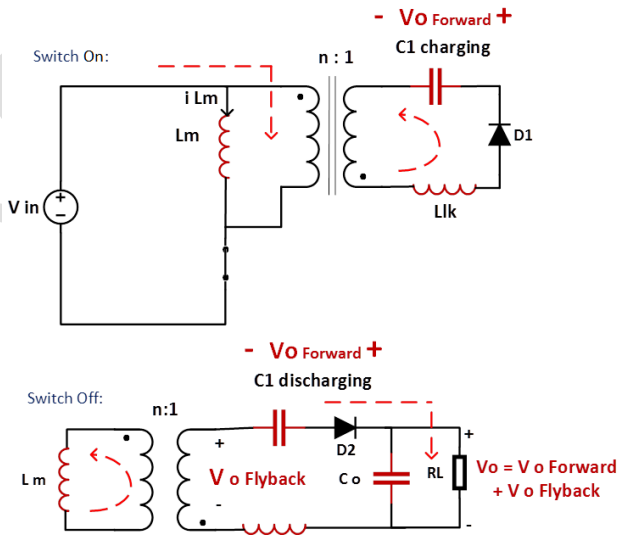

Fig. 2. Description of forward–flyback converter operation

In fact, since the forward-flyback converter is created by the combination of two forward and flyback sections, the control input to output transfer function is obtained based on the following steps:

Uncorrected Proof

- Separate the converter as drawn in Fig. 3

- Calculate the transfer function of each of the specified sections (forward section and flyback section)

- Based on the principle of superposition the transfer function of the original converter is determined as the sum of these transfer functions.

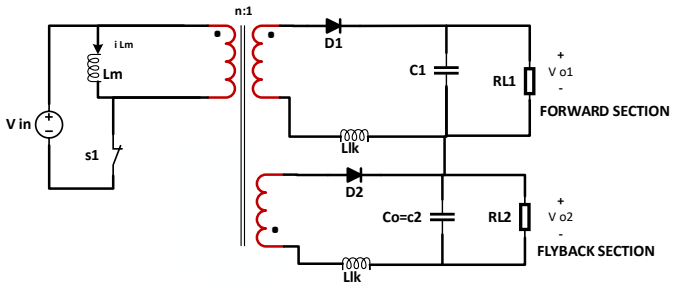

Fig. 3. Decoupled forward– flyback converter

By separating the forward-flyback converter into two forward and flyback sections; according to Fig. 3, the load resistance for each of these two sections is obtained based on the following relationships in CCM (using the voltage divider):

$$R_{L1}+R_{L2}=R_L\ ,\ V_{C1}=\frac{V_{in}}{n}$$

$$\frac{V_{in}}{n}=\frac{R_{L1}}{R_{L1}+R_{L2}}\left(V_{C1}+\frac{D}{1-D}\frac{V_{in}}{n}\right)$$

$$\frac{D}{1-D}\frac{V_{in}}{n}=\frac{R_{L2}}{R_{L1}+R_{L2}}\left(V_{C1}+\frac{D}{1-D}\frac{V_{in}}{n}\right)$$

where D is the duty-cycle in steady-state; n is the transformer ratio; R_{L1} and R_{L2} are equivalent loads in forward and flyback sections respectively to achieve the same voltage and current at the output, similar to the original circuit.

$$R_{L1}=\frac{\frac{V_{in}}{n}R_L}{\frac{V_{in}}{n}+\frac{D}{1-D}\frac{V_{in}}{n}}=\left(1-D\right)R_L \tag{1}$$

$$R_{L2}=\frac{\frac{D}{1-D}\frac{V_{in}}{n}R_L}{\frac{V_{in}}{n}+\frac{D}{1-D}\frac{V_{in}}{n}}=DR_L \tag{2}$$

2-2- The transfer function of the forward section

Fig. 4 shows the circuit of the forward section in the switch on and switch off states. The peak current of diode D1 is

10.22060/EEJ.2024.23038.5584

$$I_{pD1} = \frac{\left(\frac{v_{in}}{n} - v_{o1}\right) dT_s}{L_{lk}} \tag{3}$$

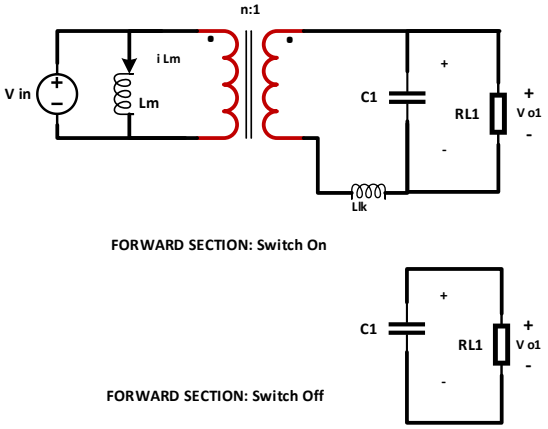

Fig. 4. Equivalent circuits of the forward section in state of switch on and switch off

where L_{lk} is the leakage inductance of the transformer; $d=D+\hat{d}$ is the duty-cycle; $\hat{d}$ is the duty-cycle perturbation; T_s is the switching period.

The average current of diode D1 is determined as follows:

$$i_{D1} = \frac{I_{pD1} d}{2} = \frac{\left(\frac{v_{in}}{n} - v_{o1}\right) d^2 T_s}{2L_{lk}} \tag{4}$$

Using Kirchhoff's current law one can obtain the output node:

$$c_1 \dot{v}_{o1} = i_{D1} - \frac{v_{o1}}{R_{L1}} \tag{5}$$

$$\dot{v}_{o1} = \frac{\left(\frac{v_{in}}{n} - v_{o1}\right) d^2 T_s}{2L_{lk}C_1} - \frac{v_{o1}}{R_{L1}C_1} \tag{6}$$

By linearizing the equations around the operating point and neglecting high-order nonlinear terms and input voltage changes; the linearized equation is obtained as follows:

$$\dot{v}_{o1} = \frac{\left(\frac{v_{in}}{n} - v_{o1}\right) d^2 T_s}{2L_{lk}C_1} - \frac{v_{o1}}{R_{L1}C_1} \tag{6}$$

$$\dot{\hat{v}}_{o1} = \left(\frac{-D^2 T_s}{2L_{lk}C_1} - \frac{1}{R_{L1}C_1}\right)\hat{v}_{o1} + \left(\frac{\frac{V_{in}}{n} 2DT_s - 2DV_{o1}T_s}{2L_{lk}C_1}\right)\hat{d} + \left(\frac{\frac{V_{in}}{n} D^2 T_s - D^2 V_{o1} T_s}{2L_{lk}C_1} - \frac{V_{o1}}{R_1 C_1}\right) \tag{7}$$

The variables with ^ symbol are the perturbations around the steady-state quantities.

Uncorrected Proof

The output variable is:

$$y = \hat{v}_{o1} \tag{8}$$

In steady state condition:

$$V_{o1} = \frac{\frac{V_{in}}{n} D^2 T_s R_{L1}}{D^2 T_s R_{L1} + 2L_{lk}} \tag{9}$$

For small signal variation conditions:

$$\hat{\dot{v}}_{o1} = A\hat{v}_{o1} + B\hat{d} \tag{10}$$

where:

$$B = \frac{\frac{V_{in}}{n} 2DT_s - 2DV_{o1}T_s}{2L_{lk}C_1} \tag{11}$$

$$A = \frac{-D^2 T_s}{2L_{lk}C_1} - \frac{1}{R_{L1}C_1} \tag{12}$$

Finally, the control input to output transfer function is:

$$F_{Forward} = \frac{2DT_s R_{L1}\left(\frac{v_{in}}{n} - V_{o1}\right)}{(D^2 T_s R_{L1} + 2L_{lk}) + 2L_{lk}C_1 s} \tag{13}$$

where *s* is the Laplace transformation variable.

By substituting V_{o1} from Eq. (9):

$$F_{Forward} = \frac{4DL_{lk}T_s R_{L1} V_{in}}{n(D^2 T_s R_{L1} + 2L_{lk})\left(D^2 T_s R_{L1} + 2L_{lk} + 2L_{lk}R_{L1}C_1 s\right)} \tag{14}$$

It can be seen from the above relationship that the transfer function of the forward part has a pole on the left half plane.

2-3- The transfer function of the flyback section

The control input to output transfer function of the flyback section of the forward-flyback converter is as follows:

$$F_{Flyback}(s) = \frac{v_{o2}(s)}{d(s)} = \frac{V_{in}}{n(1-D)^2} \frac{n^2(1-D)^2 R_{L2} - L_m Ds}{n^2(1-D)^2 R_{L2} + L_m s + L_m R_{L2} C_o s^2} \tag{15}$$

2-4- The transfer function of the Forward-Flyback converter

10.22060/EEJ.2024.23038.5584

The output voltage of the forward-flyback converter is the sum of the output voltage of the forward and flyback sections. Therefore, according to the principle of superposition, the control input to output transfer function for the forward-flyback converter is obtained from the sum of the control input to output transfer functions of the forward section and flyback section.

$$v_o = v_{o1} + v_{o2} \tag{16}$$

$$F_{ForwardFlyback}(s) = F_{Forward}(s) + F_{Flyback}(s) = \frac{V_{in}\left(P_1 + P_2 s + P_3 s^2\right)}{n(D-1)^2 Q_1 (Q_1 + Q_2 s)\left(Q_3 + L_m s + Q_4 s^2\right)} \tag{17}$$

$$P_1 = n^2\left(4L_{lk}^2(1-D)^2 + DR_{L1}T_s\left(4L_{lk}\left(1-3D\left(1+D^2\right)+D^2\left(4+D^2\right)\right)+D^3R_{L1}T_s\left(1-D+D^2\right)\right)\right) \tag{18}$$

$$P_2 = 2R_{L2}R_{L1}C_1L_{lk}n^2\left(\left(T_sR_{L1}D^2+2L_{lk}\right)(1-D)^2\right)+L_mD\left(4T_sR_{L1}L_{lk}(1-2D)-\left(4L_{lk}^2D^4R_{L1}^2T_s^2\right)\right) \tag{19}$$

$$P_3 = 2L_mR_{L1}D\left(2R_{L2}C_oL_{lk}T_s(1-D)^2 - C_1L_{lk}\left(D^2R_{L1}T_s+2L_{lk}\right)\right) \tag{20}$$

$$Q_1 = R_{L1}T_sD^2 + 2L_{lk} \tag{21}$$

$$Q_2 = 2L_{lk}R_{L1}C_1 \tag{22}$$

$$Q_3 = R_{L2}n^2(1-D)^2 \tag{23}$$

$$Q_4 = L_mR_{L2}C_o \tag{24}$$

where L_m is the magnetizing inductance of the transformer.

To validate the obtained new modeling of the forward-flyback converter, small AC signals with three frequencies are considered in the duty-cycle and the output voltages of the converter circuit and the obtained model are shown in Figs. 5.a and 5.b respectively. It can be seen the responses are almost the same. The small differences are from the switching effects, the approximation in the modeling and the calculation errors.

The forward-flyback converter has three stable poles and two zeros in its transfer function, one of these zeros is on the left half plane, and the second zero can be placed on the left half plane or RHP based on the values of the converter parameters. Therefore, the forward-flyback converter, unlike the flyback converter, can be the minimum phase for some values of its circuit parameters.

Uncorrected Proof

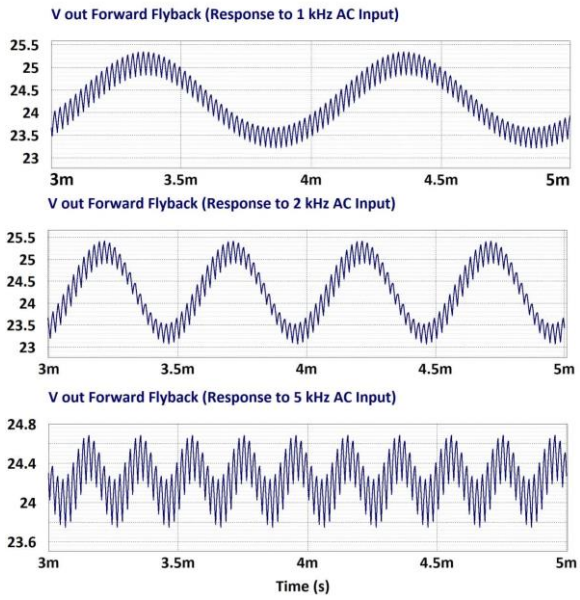

(a)

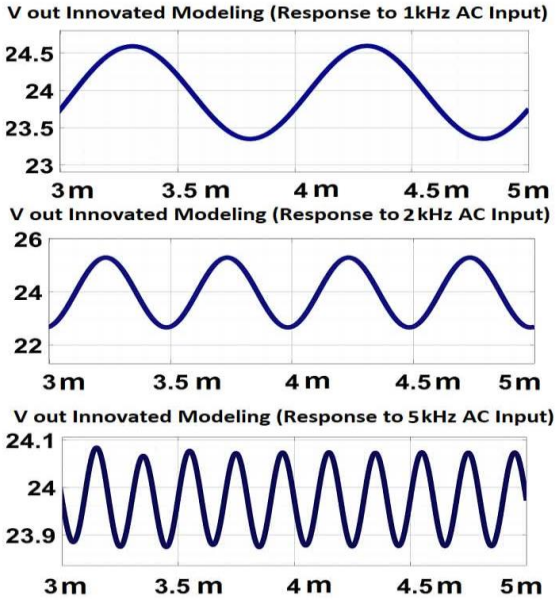

(b)

Fig. 5. Small AC (frequency) responses a) responses from forward-flyback circuit converter b) responses from forward-flyback model

3. Calculation of forward-flyback converter transformer

If the operation of the converter in the CCM is considered, the current of the magnetizing inductor will be almost constant:

$$I_{Lm} = I_1 \tag{25}$$

The average current of diode D_2 is equal to the average output current:

$$I_o = I_{D2} \tag{26}$$

On the other hand, due to the current balance of the second capacitor, the average current of diode D_1 is also equal to the output current:

$$I_o = I_{D1} \tag{27}$$

In the switch on state, the primary voltage of the transformer is equal to the input voltage. The output voltage is related to the input voltage by the transformation ratio of the transformer. The voltage of the capacitor C1 will be equal to the secondary voltage:

$$V_p = V_{in} \tag{28}$$

$$V_s = V_{C1} = \frac{V_{in}}{n} \tag{29}$$

Based on the balance of the secondary voltage in the magnetizing inductor of the transformer in a complete cycle:

$$V_{in}D = (V_o - V_{C1})n(1-D) \tag{30}$$

10.22060/EEJ.2024.23038.5584

Finally, the output voltage of the forward-flyback converter is obtained as follows:

$$V_o \cong \frac{V_{in}D + nV_{C1}(1-D)}{n(1-D)} \tag{31}$$

Fig. 6 shows the waveform of the input current and diode D_2 current in a cycle. The load corresponding to level A in the secondary causes the capacitor C1 to be charged, so the average current corresponding to level A will be equal to I_O / n and based on the balance of the second current in the secondary capacitor, the average input current is obtained as follows:

$$I_{in} = \frac{1}{T_s}(A+B) = \frac{1}{T_s}A + \frac{1}{T_s}B = \frac{I_o}{n}n + I_1 D \tag{32}$$

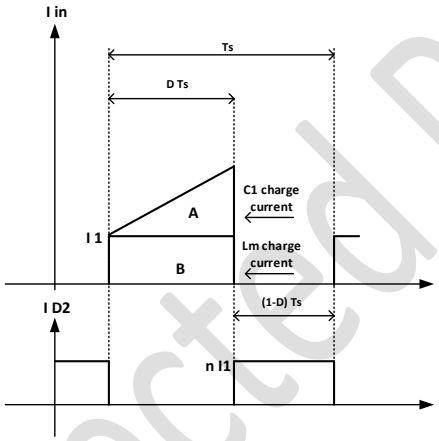

Fig. 6. Waveform of input current and output diode in one period

According to Eq. (26), the average current of diode D_2 is equal to the average output current, therefore:

$$nI_1(1-D) = I_o \tag{33}$$

$$I_1 = I_{Lm} = \frac{I_o}{n(1-D)} \tag{34}$$

The average value of output current in terms of output power is equal to:

$$I_o = \frac{P_o}{V_o} \tag{35}$$

The maximum magnetizing current is obtained by considering the current ripple of the magnetizing inductor as follows:

$$I_{Lm\,max} = I_1 + \frac{1}{2}\frac{V_{in}}{L_m}DT_s \tag{36}$$

Uncorrected Proof

To remain in the CCM, the following condition must be satisfied:

$$\frac{V_{in}}{L_m} DT_s < 2I_1 \tag{37}$$

After determining the value of the magnetizing inductance and the maximum magnetizing current of the transformer, the number of primary turns of the transformer will be calculated from:

$$L_m I_{Lm\,max} = N_p BA \tag{38}$$

where N_p is the number of turns in the transformer primary; B is the flux density; A is the cross-section area of the core.

4. Design of the minimum phase forward-flyback converter in CCM

Unlike the flyback converter, which has a RHP zero in all ranges of the duty cycle and transformer ratio of the transformer which has a non-minimum phase nature; the forward-flyback converter can be minimum phase with some duty cycles and transformer ratios. To design a minimum phase forward-flyback converter in CCM, it is necessary to perform the design steps of the converter according to Fig. 7. Based on the algorithm illustrated in Fig. 7, a forward-flyback converter with the general specifications stated in Table 1 has been designed. The minimum and maximum range for the transformer ratio is between 1 and 10 and the duty cycle is from 1 to 90%. Reducing the size of the magnetizing inductance of the transformer (L_m), leads to the improvement of the minimum phase effect of the converter. Also, to keep the converter in the CCM, it is necessary to consider a minimum value for L_m based on the condition Eq. (37). According to this, it is suggested to choose a double confidence margin for choosing L_m.

To design the forward-flyback converter in the CCM with the condition of minimum-phase dynamic behavior, the magnetizing inductance value of the transformer is first determined. It is also necessary to determine the values of the turn ratio and the leakage inductance of the transformer coil, therefore, based on the flowchart in Fig. 7, first, the minimum value of the magnetization inductance is determined by considering a suitable margin so that the condition Eq. (37) is met. Then the amount of leakage inductance is experimentally determined according to the coupling coefficient and a range is also selected for the values of the turn ratio and the duty factor. The minimum-phase region of the converter is determined for different values of n and D according to the previously determined values of Lm and Llk and based on the zeros of the converter transfer function. Also, in this minimum-phase region, the values that set the output voltage of the converter at the nominal value are also determined. Then, from this area, the maximum values of n and D are selected so that the converter has less stress on the switch. Now, because the selected value of n

10.22060/EEJ.2024.23038.5584
and *D* changes the condition Eq. (37), the value of *Lm* is updated again. Therefore, so far the values of *Lm* and *n* have been finalized and the value of *Llk* should also be measured after the construction of the transformer. Finally, by designing the transformer based on the values of *Lm* and n and measuring the value of *Llk* after its construction, the final value of the duty cycle that results the rated operating point of the converter is determined.

Table 1. General specifications of forward-flyback converter

Power	50 W
Input voltage	150 v
Rated output voltage	24 v
Switching frequency	50 kHz
Capacitor of the Forward sec. C1	100 µF
Output capacitor C_o	47 µF

For the initial design of the converter, considering that the leakage inductance value of the transformer is not yet known, this value is considered based on the estimated value of the coupling coefficient equal to ten percent of L_m. Then the transformer ratio and the duty cycle are obtained so that the converter remains in the minimum phase zone and satisfies the voltage gain equation. The minimum value of L_m required for the converter to remain in CCM, considering a sufficient margin for transformer ratio and different duty cycles is shown in Fig. 7. Fig. 8 shows the range of transformer ratios and duty cycles that provide the converter minimum phase and non-minimum phase zones.

Uncorrected Proof

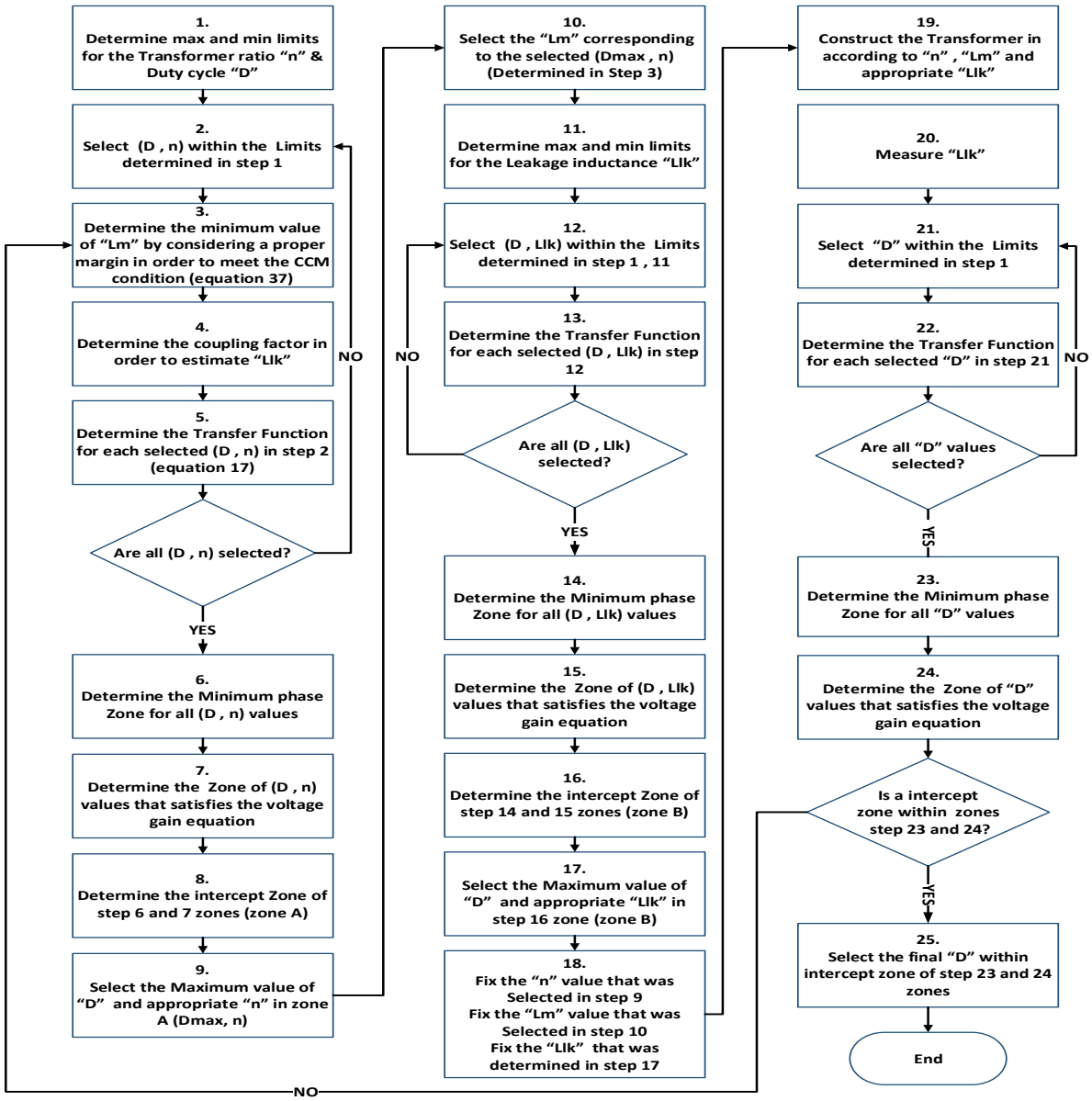

Fig. 7. Flowchart of forward-flyback converter design without RHP zeros

Notably, all the points of this range do not satisfy the voltage gain equation, so in Fig. 10 range of these points satisfied in the voltage gain equation is shown. Finally, the intersection of the above two zones, which satisfies both conditions of being minimum phase and the voltage gain equation in the CCM are shown in Fig. 10. These points are listed in Table 2.

To reduce the effective value of current and switch stress, it is better to choose the highest possible duty cycle for the converter. Therefore, based on the results of Table 2, the most appropriate choice for the converter is the transformer ratio equal to 9 and the duty cycle equal to 50% (Assuming that the leakage inductance is a certain percentage of the magnetization inductance).

The next step is to construct the transformer, which must be wound based on the transformer ratio of 9 and the magnetizing inductance of 2.9 mH. By choosing the ferrite core of type EE42/21/20 and according to Eq. (38), the

10.22060/EEJ.2024.23038.5584
number of primary turns of the transformer is equal to 63 turns and the number of secondary turns is calculated to be equal to 7 turns.

After winding the transformer and setting the magnetizing inductance to 2.9 mH, the leakage inductance of the transformer winding is measured. The maximum and minimum range for the leakage inductance value of the transformer is experimentally considered between 1 and 10 μH.

The minimum phase zone of the converter is determined by selecting the duty cycle and the leakage inductance in the defined zone (Fig. 11). The zone where the voltage gain equation is satisfied is shown in Fig. 12. Values of duty cycle and leakage inductance that satisfy both minimum phase zone and voltage gain conditions are obtained by subscripting these two zones (Fig. 12).

Table 3 shows the values of leakage inductance and the corresponding duty cycle. If the winding of the transformer is implemented properly, it is possible to achieve low values of leakage inductance. Increasing the value of the leakage inductance leads to increasing the duty cycle to reach the nominal operating point, and its excessive can result in a non-minimum phase zone (Fig. 12).

Table 2. The values of transformer ratio and duty cycle satisfying all three conditions of CCM, voltage gain and minimum phase

Duty cycle	Transformer ratio
% 20	3
% 30	5
% 40	7
% 50	9

On the other hand, with a large increase in leakage inductance, the duty cycle needs to be increased to satisfy the voltage gain equation, which causes the converter to go towards the non-minimum phase zone. The design of the transformer is completed by winding the transformer properly and measuring the actual value of the leakage inductance of the winding. Based on the results obtained from the implementation of the algorithm presented in this paper, the selected values for the forward-flyback converter to operate in the continuous conduction mode and to be within the minimum phase zone are given in Table 4.

Table 3. The values of leakage inductance and duty cycle satisfying both conditions of voltage gain and minimum phase

Duty cycle	Leakage inductance (μH)	Duty cycle	Leakage inductance (μH)

Uncorrected Proof

48 %	1	54.5%	6
50 %	2	55%	7
52 %	3	55.2%	8
53 %	4	55.5%	9
54 %	5	56%	10

Table 4. Final design values of minimum phase forward-flyback converter in CCM mode

Input voltage	150 v
Power	50 W
Rated output voltage	24 v
Core magnetization inductance	2.9 mH
The leakage inductance of winding	7 µH
Primary to secondary circuit ratio	9
Nominal duty cycle	55 %

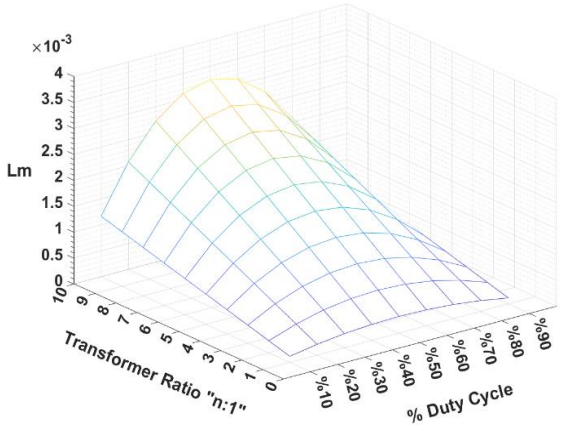

Fig. 8. Determination of Lm for the minimum phase condition and CCM

The flyback converter is non-minimum phase for all duty cycles, and increasing the duty cycle in this converter intensifies the effect of being non-minimum phase. This causes RHP zero to approach the origin. Based on the

10.22060/EEJ.2024.23038.5584
analysis done in the fourth section, the maximum duty cycle that the forward-flyback converter remains minimum phase is 57%. The nominal duty cycle considered for this converter is considered to be 55%. The location of the zeros and poles of the forward-flyback converter designed according to the parameters of Table (4) is shown in Fig. 13.

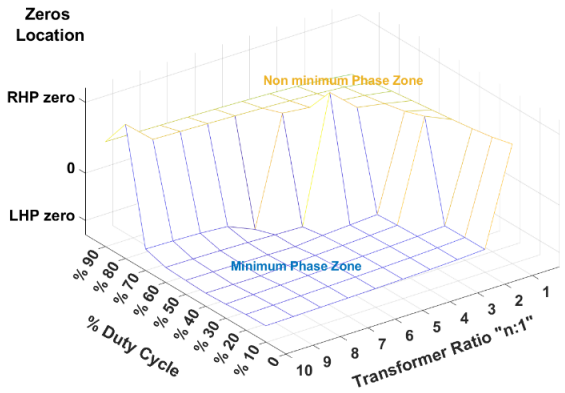

Fig. 9. Determination of minimum phase zone for the range of Transformer ratio and duty cycle

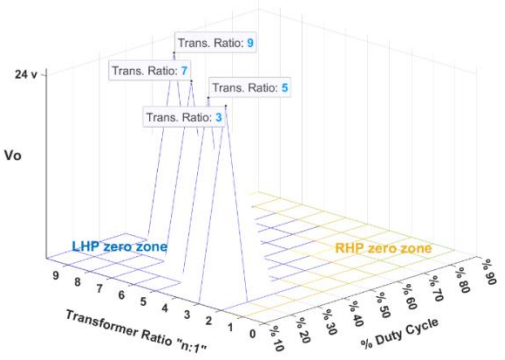

Fig. 10. Determination of the range of transformer ratio and duty cycles for satisfying voltage gain equation and minimum phase condition

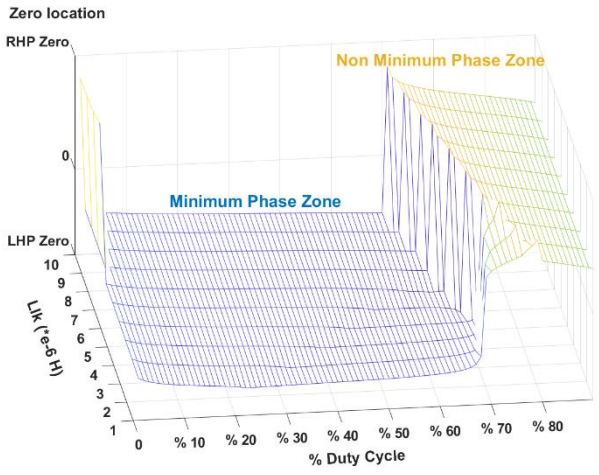

Fig. 11. Determination of minimum phase zone for the range of duty cycle and leakage inductance

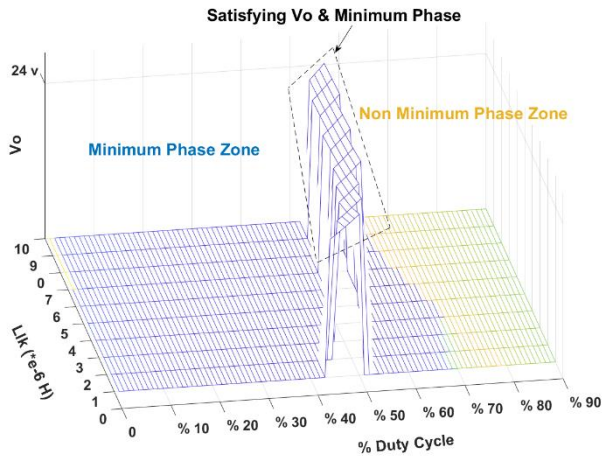

Fig. 12. Determination of values of duty cycle and leakage inductances that satisfy both minimum phase condition and voltage gain equation

By changing the output power of the converter, the duty cycle of the converter changes, so the converter must remain in the minimum phase zone in the condition of changing the output power. Fig. 14 shows a range of converter duty cycles that satisfy the gain voltage equation at different output powers. The design method presented in this paper guarantees the remaining of the converter in the minimum phase zone for output power changes (Fig. 14).

In fact, unlike the flyback converter, which inherently has a zero in the control input to output transfer function for all duty cycles, and it appears on RHP; the zeros of this converter can be placed on the left half plane for some parameters and duty cycles. In other words, minimum phase dynamic behavior is possible for the forward-flyback converter. Fig. 15 depicts the bode diagrams of the forward and flyback sections and the forward-flyback converter. It can be seen that the flyback converter is always non-minimum phase; the forward converter is always minimum phase and the forward-flyback converter is minimum phase. Fig. 16 shows the dynamic behavior of the output voltage of both flyback and forward-flyback converters with changes in the output voltage from 24 to 12 volts. It is seen that the behavior of the flyback converter is non-minimum phase, while the behavior of the forward-flyback converter is minimum phase.

AUT Journal of Electrical Engineering
10.22060/EEJ.2024.23038.5584

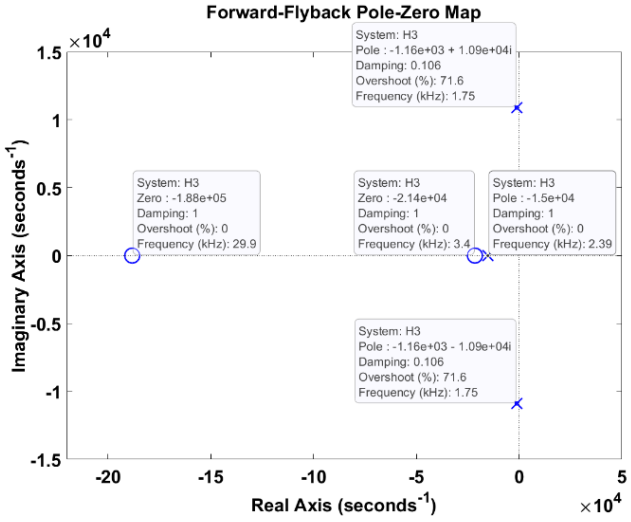

Fig. 13. Location of the zeros of the transfer function of the forward-flyback converter with changes in the duty cycle

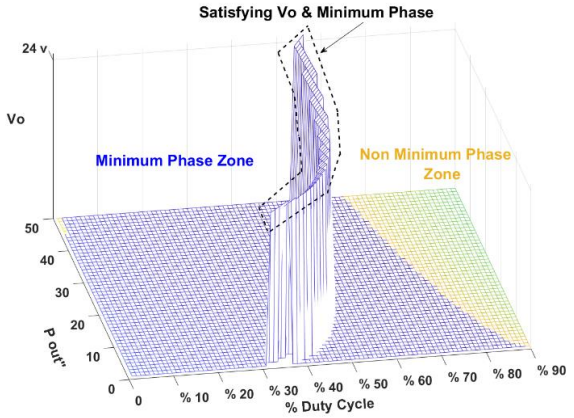

Fig. 14. The range of converter duty cycles for satisfying the gain voltage equation at different output powers

Uncorrected Proof

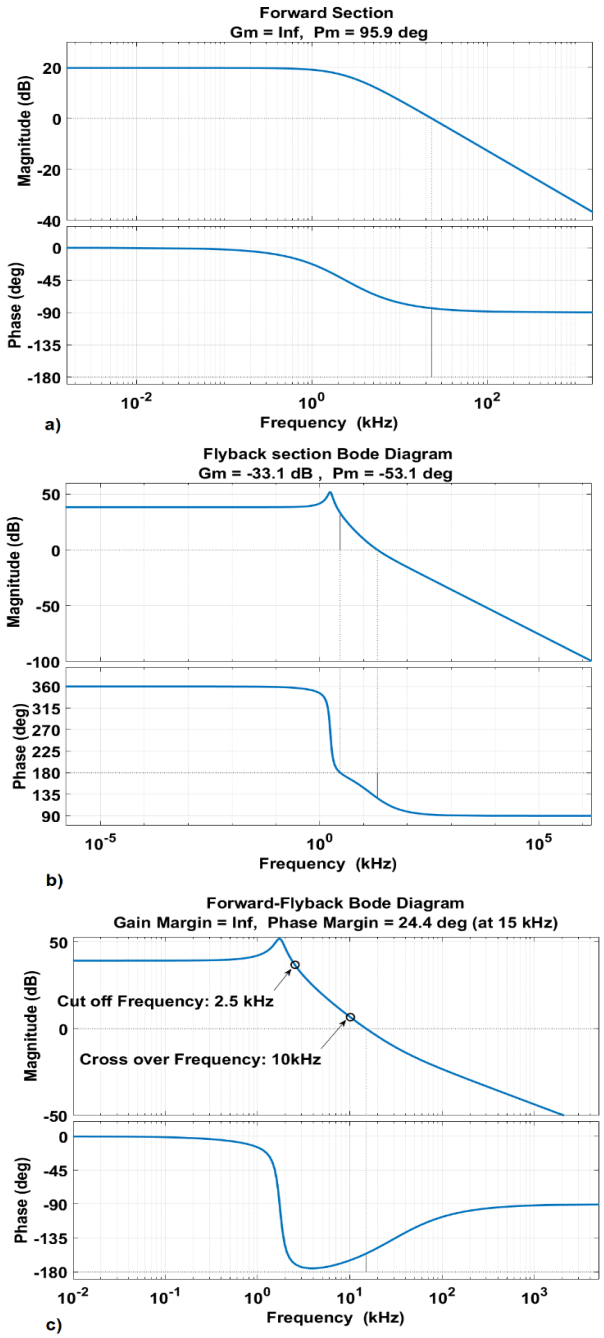

Fig. 15. Bode diagram a) forward section, b) flyback section and c) forward-flyback converter

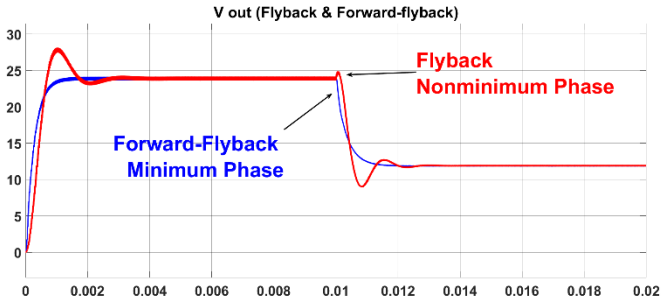

Fig. 16. Output voltage of flyback and forward-flyback converters

10.22060/EEJ.2024.23038.5584

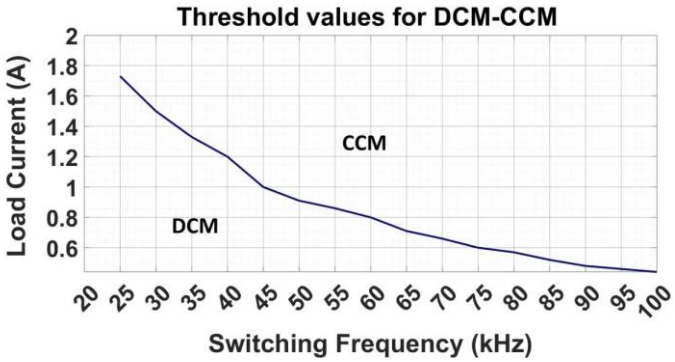

Fig. 17. The CCM and DCM regions of forward-flyback converter with the designed converter specifications

Fig. 17 shows the CCM and DCM regions of forward-flyback converter considering the load current and the switching frequency with the designed converter specifications.

To compare the flyback, forward and forward-flyback converters, some aspects of these converters are presented in Table 5. In this table N_1 and N_3 are the number of turns in primary and demagnetizing windings; i_m is the magnetizing current; i_2 is the transformer secondary current which can be larger for forward-flyback converter compared to forward converter because of the charging current of the series capacitor.

Table 5. Some aspects of flyback, forward and forward-flyback converters

	voltage gain in CCM	number of capacitors	number of diodes	number of inductors	number of transformers	input current	Power switch voltage stress
flyback converter	$\frac{D}{1-D}\frac{1}{n}$	1	1	0	1	i_m	$V_{in}+nV_o$
forward converter	$D\frac{1}{n}$	1	1	1	1	$i_m+\frac{i_2}{n}$	$V_{in}+\frac{N_1}{N_3}V_{in}$
Forward-flyback converter	$\frac{1}{1-D}\frac{1}{n}$	2	2	0	1	$i_m+\frac{i_2}{n}$	$V_{in}+n(V_o-\frac{V_{in}}{n})$ $=nV_o$

5. Feedback compensation circuit design

5-1- Feedback control loop

Uncorrected Proof

To control and regulate the output voltage of the forward-flyback converter, a voltage control loop is used. A general solution for unconditional stability for CCM operation of the converter in voltage mode with any type of output capacitor and a wide range of ESR values is to use a feedback control loop with a type III compensating circuit [37]. The transfer function of the compensating circuit used in this loop has two zeros and three poles, one of which is located at the origin. The block diagram of the feedback control loop and the circuit model along with the compensator gain diagram are shown in Fig. 18.

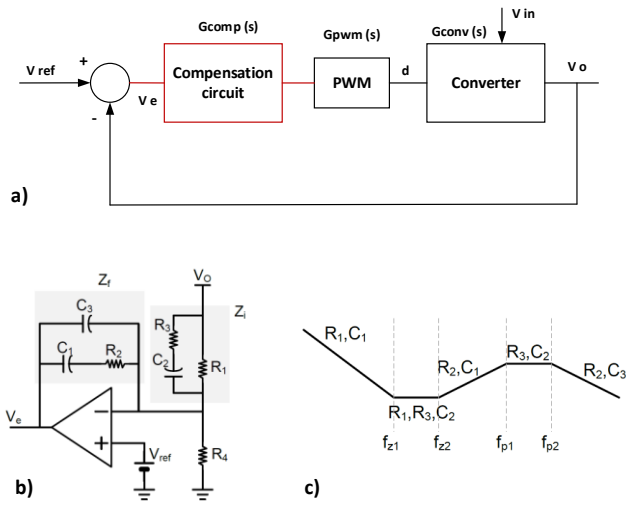

Fig. 18. Feedback control loop a) block diagram b) circuit model c) gain diagram

In general, the efficiency and stability of the voltage control loop to adjust the output voltage of the converter are determined based on the open loop characteristics of the system. In this compensator, the combination of capacitor C3 and R2 creates a pole and the combination of C_1 and R_2 creates a zero, assuming that the frequency of the pole is higher than zero (C_1>>C_3), the transfer function of the compensator is as follows:

$$H(s)=\frac{Z_f}{Z_i}\approx\frac{\left(sC_2\left(R_1+R_3\right)+1\right)\left(sC_1R_2+1\right)}{\left(sR_1C_1\right)\left(sC_2R_3+1\right)\left(sR_2C_3+1\right)} \tag{39}$$

The frequency of the poles and zeros of the compensator is as follows [37]:

$$f_{p0}=\frac{1}{2\pi R_1\left(C_1+C_3\right)}\approx\frac{1}{2\pi R_1C_1} \tag{40}$$

$$f_{p1}=\frac{1}{2\pi R_3C_2} \tag{41}$$

$$f_{p2}=\frac{1}{2\pi R_2}\left(\frac{1}{C_1}+\frac{1}{C_3}\right)\approx\frac{1}{2\pi R_2C_3} \tag{42}$$

10.22060/EEJ.2024.23038.5584

$$f_{z1} = \frac{1}{2\pi\left(R_1 + R_3\right)C_2} \tag{43}$$

$$f_{z2} = \frac{1}{2\pi R_2 C_1} \tag{44}$$

By selecting a value for R_1 and correctly placing the poles and zeros of the compensator according to the desired specifications, the transfer function of the forward-flyback converter whose calculation method is explained in this paper, the values of the capacitors and the resistances of the compensator circuit are determined. The open loop gain of the feedback control is as follows:

$$G_{OL}(s) = G_{comp}(s) \times {}^{1}\!/_{V_{osc}} \times G_{conv}(s) \tag{45}$$

where *Vosc* corresponds to the peak amplitude of the sawtooth waveform of the PWM section; G_{comp} is the compensator transfer-function and G_{conv} is the converter transfer-function. To achieve a small steady state error between the output voltage of the converter and the reference voltage; the gain should be high at low frequencies but small at the switching frequency. In the design of the compensation circuit and the placement of zero and its poles, the crossover frequency (f_c) of the converter plays an important role. Normally, this frequency is selected for switching converters between a quarter and a tenth of the switching frequency to enable quick response to disturbances.

The bode diagram obtained from the transfer function of the forward-flyback converter (with the specifications of Table 4) whose calculation method was described in this paper is given in Fig. 15c. Also, the frequency of poles and zeros of the converter is given in the table 6.

Table 6. Location and frequency of converter poles and zeros

	Location	Frequency (kHz)
Pole1	-1.16e3 + j1.09e4	1.75
Pole2	-1.16e3 - j1.09e4	1.75
Pole3	-1.5 e4	2.39
Zero1	-2.14e4	3.4
Zero2	-1.88e5	29.9

Uncorrected Proof

5-2- Compensator circuit design

The phase margin at the frequency of 15 kHz is 24.4^{O}, which must be increased by the compensator circuit to ensure the stability of the system. Because the first pole of the compensator is located at the origin, the first zero of the compensator must be at a frequency lower than the pair of converter poles so that the phase of the loop does not tend to zero near this frequency. A suitable choice for the first zero of the compensator circuit is as follows [37]:

$$f_{z1} \approx 0.7 \times f_{pp} \tag{46}$$

where f_{pp} is the frequency of the complex conjugate poles of the converter.

According to Table 5, the frequency of the pair of converter poles is 1.75 kHz, so the first zero frequency of the compensator is selected as 1.2 kHz. The second zero of the compensator should compensate the other pole of the converter so that the loop gain slope at the gain pass frequency is -20 dB/dec. Considering that the gain pass frequency of the converter is 15 kHz, the second zero frequency of the compensator is determined to be 16 kHz. The second pole of the compensator should be at a frequency higher than the crossover frequency and lower than the switching frequency (f_{sw}) so that lag does not reduce the phase margin, so it is better to determine the frequency of the second pole as follows [37]:

$$f_{P2} \approx \frac{f_{sw}}{2} \tag{47}$$

Therefore, the frequency of the second pole is also chosen to be 25 kHz. The third pole of the compensator should provide more attenuation for high frequencies, so the frequency of the third pole is close to the second zero frequency of the converter and equal to 40 kHz. Also, the gain of the loop at the crossover frequency must be unity, that is:

$$\left| G_{comp}(s) \times \frac{1}{V_{osc}} \times G_{conv}(s) \right| = 1$$

Fig. 19 is the bode diagram of the feedback control open loop. The frequency of the pole and zeros of the compensator are given in Table 7.

One of the main purposes of this paper was the design of the minimum phase forward-flyback converter in CCM mode, which was done in the previous section. The diagram of Fig. 19 shows that the converter is minimum phase.

As shown in Fig. 19, the minimum phase condition of the system is maintained. The phase margin tends to infinity after compensation. Also, the gain and phase margin at the crossover frequency have increased after compensation.

10.22060/EEJ.2024.23038.5584
After compensation, the cutoff frequency is increased from 2.56 kHz to 3.82 kHz, and thus the bandwidth of the system after compensation is increased. On the other hand, the cutoff rate of the open-loop transfer function has become slower, which is desirable. Also, the gain in low frequencies has increased.

Table 7. Location and frequency of compensator poles and zeros

	Location	Frequency (kHz)
Pole2	-1.57e5	25
Pole3	-2.51e5	40
Zero1	-7.54e3	1.2
Zero2	-1.01e4	16

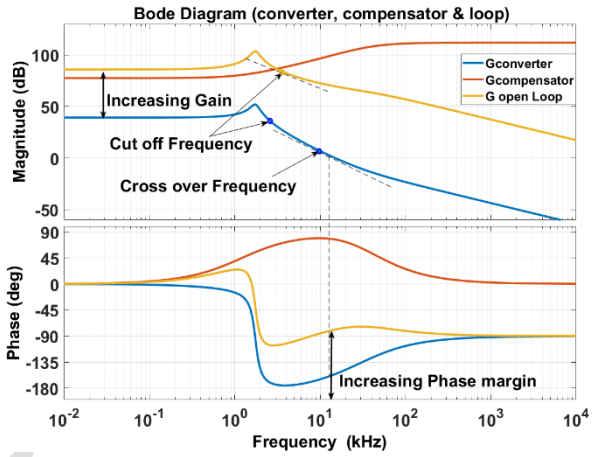

Fig. 19. The Converter, compensator and open loop Bode diagram

Fig. 20 shows the step response of the converter along with the step response after placing the compensator in the feedback control loop. According to Fig. 20, the step response of the output voltage of the converter controlled by the feedback loop has better transient behavior and has reached the reference voltage in less time.

The effectiveness of the designed feedback loop in following the output voltage in the condition of changing the load current from 50% to 100% of the nominal and changing the reference voltage is shown in Fig. 21. Of course, it is certain that if the feedback loop is not used, it will not be possible to track the reference voltage due to the change of the operating point.

Uncorrected Proof

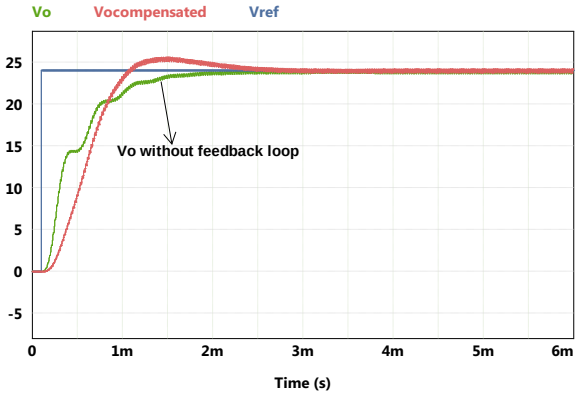

Fig. 20. The step response of the forward-flyback converter (with & without feedback loop)

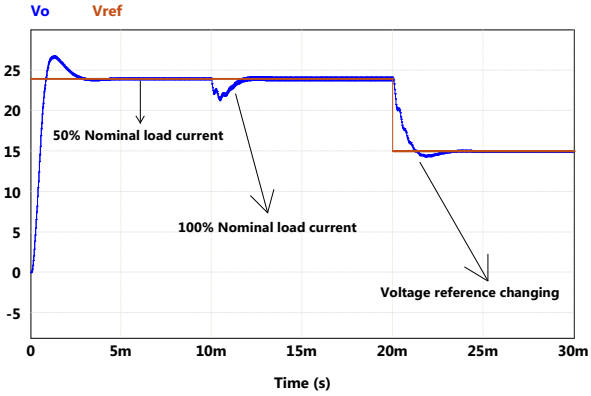

Fig. 21. The output voltage transient behavior

5-3- Nonlinear controller design and simulation

In this section, a nonlinear controller is designed for forward-flyback converter based on the proposed equivalent circuit shown in Fig. 3. Taking the time derivative of Eq. (16) and considering the average models of forward and flyback sections, one can obtain:

$$\frac{dv_o}{dt} = f(d) + g \tag{48}$$

where:

$$f(d) = \frac{(1-d)ni_{L_m}}{c_o} + \frac{\left(\frac{v_{in}}{n} - v_{o1}\right)d^2T_s}{2L_{lk}c_1} \tag{49}$$

$$g = -\frac{v_{o1}}{R_{L1}c_1} - \frac{v_{o2}}{R_{L2}c_o} \tag{50}$$

Define the following output voltage error:

$$h = v_o - \overline{v_o} \tag{51}$$

10.22060/EEJ.2024.23038.5584

where $\overline{v_o}$ is constant output voltage reference.

Taking the time derivative of Eq. (51) and using Eq. (48), the following error dynamics is obtained:

$$\dot{h} = \dot{v}_o = f(d) + g \tag{52}$$

To achieve a fast convergence of error to zero, the following dynamics proposed:

$$\dot{h} = -K_1 h - K_2 sign(h) - K_3 \int_0^t h dr \tag{53}$$

where K_1, K_2 and K_3 are positive constants which are tuned by trial and error.

Comparing Eq. (52) with Eq. (53), yields:

$$f(d) = -g - K_1 h - K_2 sign(h) - K_3 \int_0^t h dr \tag{54}$$

In fact, Eq. (54) is the control law. The proposed control is a combination of nonlinear feedback linearization control and sliding mode control with an integral term. Using Eqs. (54), (49) and (50), the duty cycle is obtained from the following quadratic equation:

$$ad^2 + bd + c = 0 \tag{55}$$

where:

$$a = \frac{\left(\frac{v_{in}}{n} - v_{o1}\right) T_s}{2 L_{lk} c_1} \tag{56}$$

$$b = -\frac{n i_{L_m}}{c_o} \tag{57}$$

$$c = \frac{n i_{L_m}}{c_o} + g + K_1 \mathrm{h} + K_2 \mathrm{sign}(h) + K_3 \int_0^t h dr \tag{58}$$

To verify the obtained model and the effectiveness of the proposed control, a closed-loop control simulation test is done. In this simulation test, the voltage reference is 20v and it is changed to 24v after t=0.05s. The obtained results are shown in Fig. 22. It is seen that the output voltage tracks its reference with good dynamic. In addition, the magnetizing current and C1 voltage are within acceptable ranges. The duty cycle is also shown in Fig. 22 which is averaged in minimum-phase region.

Uncorrected Proof

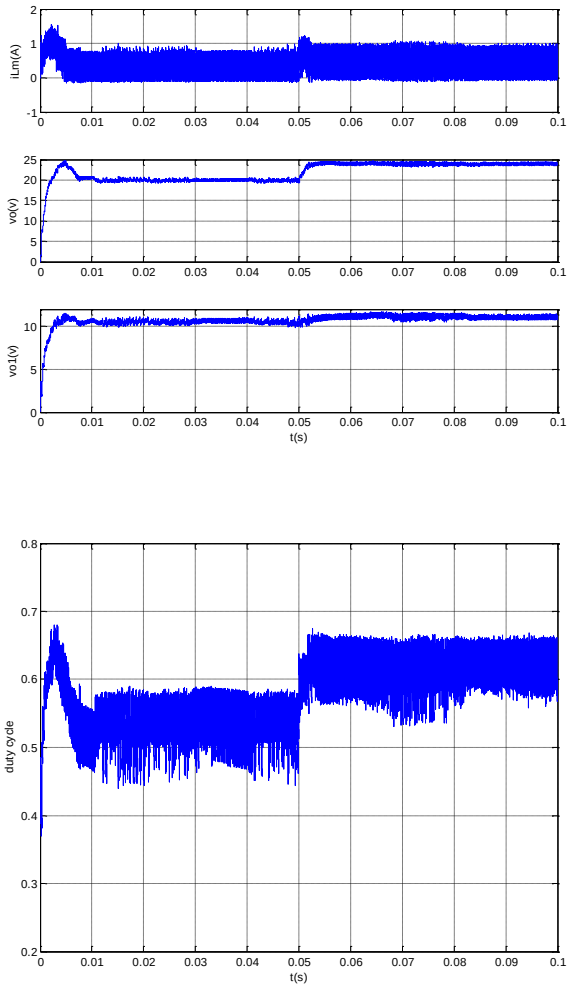

Fig. 22. Magnetizing current, output voltage, C1 voltage and the duty cycle in forward-flyback converter with the closed-loop proposed control

6. The results of the practical implementation of the forward-flyback converter and its comparison with the flyback converter

To practically evaluate the dynamic behavior of the forward-flyback converter, a laboratory prototype of flyback and forward-flyback converters has been made. Fig. 23 shows the photograph of this laboratory prototype. To verify the performance of the forward-flyback converter, the duty cycle of the converter has been changed by a step change using a signal generator.

To minimize the amount of leakage inductance of the transformer, the transformer is wound in a sandwich form, and the distances between the coils have been removed and they are completely wrapped together. The switch used in the converter is MOSFET IRF840. Fig. 24 shows the output voltage of the flyback converter for output voltage change from 12 to 24 volts. Corresponding to the flyback converter, in Fig. 25, the output voltage of the forward-flyback converter is shown for output voltage change from 12 to 24 volts.

10.22060/EEJ.2024.23038.5584

As it is known, due to the addition of a forward section, the forward-flyback converter can create the desired output voltage at a lower duty cycle compared to the flyback converter. Also, if the duty cycle range of the forward-flyback converter is less than 50%, the converter is minimum-phase and shows a better dynamic response compared to the flyback converter. Fig. 26 shows the voltage across the switch in the forward-flyback converter. A clamp circuit has been used to eliminate the severe voltage spike. As shown, adding a clamp circuit has limited the spike amplitude.

The voltages across the diodes D_1 and D_2 in a switching cycle are shown in Figs. 27 and 28 respectively. Also, in Fig. 29 the voltage across capacitor C_1 in a switching cycle is shown.

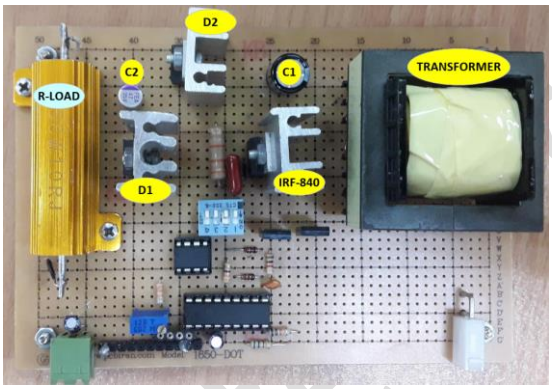

Fig. 23. Practical laboratory circuit of flyback and forward-flyback converter

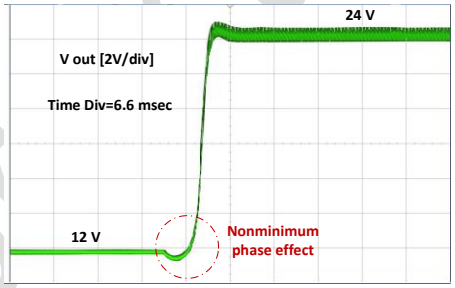

Fig. 24. Output voltage of the flyback converter

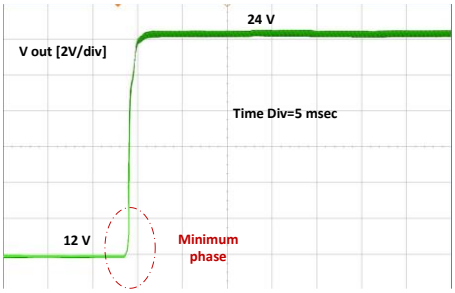

Fig. 25. Output voltage of forward-flyback converter

Uncorrected Proof

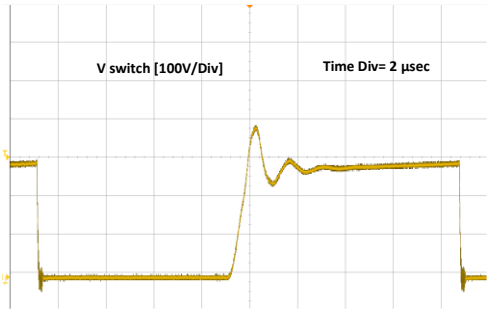

Fig. 26. Switch voltage in forward-flyback converter with clamp circuit

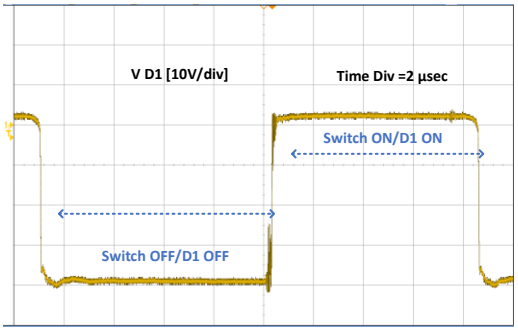

Fig. 27. D1 voltage in forward-flyback converter

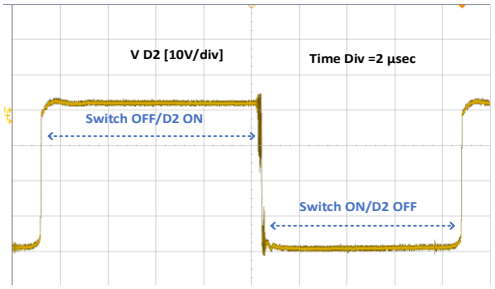

Fig. 28. D2 voltage in forward-flyback converter

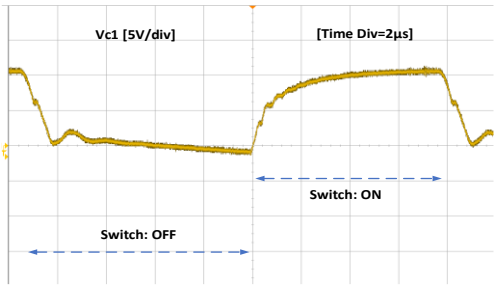

Fig. 29. C1 voltage in forward-flyback converter

7. Conclusion

In this paper, the dynamic behavior of the forward-flyback converter compared to the flyback converter is investigated. For similar input and output voltage values and power, the forward-flyback converter shows better dynamics in a range of duty cycles. To determine the transfer function of the forward-flyback converter, a new method is presented, based on which the converter is divided into two sections, flyback and forward section, and the

transfer function of each is determined separately, finally the total transfer function is calculated. Using the new modeling method, without obtaining the full order average model of the converter which has singularity for the leakage inductance of the transformer, an accurate model is obtained which is suitable for converter analysis and control design. Also, a flowchart for the design of the forward-flyback converter in minimum phase region in continuous conduction mode is presented. Simulation and experimental results represent the superiority of the forward-flyback converter over the flyback converter for some duty cycles and confirm the presented analysis. The obtained equivalent circuits, model and bode diagram can be used not only for analysis but also for control design. Based on the obtained transfer function the converter, two closed-loop control systems, using the classical control approach and nonlinear control, are designed which have appropriate performance in regulating the output voltage and validate the proposed model of the converter. It is notable that when the duty cycle falls within a specific range, the flyback-forward converter exhibits minimum phase behavior, in the next research work the converter topology is modified to extend the minimum-phase region.

References

[1] R.W. Erickson, D. Maksimovic, Fundamentals of power electronics, Springer Science & Business Media, 2007.
[2] M.K. Kazimierczuk, S.T. Nguyen, Small-signal analysis of open-loop PWM flyback dc-dc converter for CCM, in: Proceedings of the IEEE 1995 National Aerospace and Electronics Conference. NAECON 1995, IEEE, 1995, pp. 69-76.
[3] M. Sucu, Parametric average value modeling of Flyback converters in ccm and dcm including parasitics and snubbers, University of British Columbia, 2011.
[4] R. Tymerski, V. Vorperian, Generation, classification and analysis of switched-mode DC-to-DC converters by the use of converter cells, in: INTELEC'86-International Telecommunications Energy Conference, IEEE, 1986, pp. 181-195.
[5] S. Cuk, R. Middlebrook, A general unified approach to modelling switching DC-to-DC converters in discontinuous conduction mode, in: 1977 IEEE power electronics specialists conference, IEEE, 1977, pp. 36-57.
[6] V. Vorpérian, Simplified analysis of PWM converters using model of PWM switch. II. Discontinuous conduction mode, IEEE Transactions on Aerospace and Electronic systems, 26(3) (1990) 497-505.
[7] D. MaksimoviC, S. Cuk, A unified analysis of PWM converters in discontinuous modes, IEEE Transactions on Power Electronics, 6(3) (1991) 476-490.
[8] J. Sun, D.M. Mitchell, M.F. Greuel, P.T. Krein, R.M. Bass, Averaged modeling of PWM converters operating in discontinuous conduction mode, IEEE Transactions on power electronics, 16(4) (2001) 482-492.
[9] C.-C. Kuo, J.-J. Lee, Y.-H. He, J.-Y. Wu, K.-H. Chen, Y.-H. Lin, S.-R. Lin, T.-Y. Tsai, A dynamic resonant period control technique for fast and zero voltage switching in GaN-based active clamp flyback converters, IEEE Transactions on Power Electronics, 36(3) (2020) 3323-3334.
[10] S. Xu, X. Kou, C. Wang, W. Sun, L. Shi, New digital control method for improving dynamic response of synchronous rectified PSR flyback converter with CCM and DCM modes, IEEE Transactions on Power Electronics, 35(11) (2020) 12347-12358.
[11] J.-p. Qiu, L.-n. He, Y.-l. Wang, A multimode digital controller IC for flyback converter with high accuracy primary-side feedback, Journal of Zhejiang University SCIENCE C, 14 (2013) 652-662.
[12] Y. Li, J. Zheng, A low-cost adaptive multi-mode digital control solution maximizing AC/DC power supply efficiency, in: 2010 Twenty-Fifth Annual IEEE Applied Power Electronics Conference and Exposition (APEC), IEEE, 2010, pp. 349-354.
[13] S. Xu, D. Ni, S. Lu, W. Sun, A novel digital multi-mode control strategy with PSM for primary-side flyback converter, International Journal of Electronics, 104(5) (2017) 840-854.
[14] T. Chen, W. Lin, C. Liaw, Dynamic modeling and controller design of flyback converter, IEEE Transactions on aerospace and electronic systems, 35(4) (1999) 1230-1239.
[15] F.F. Edwin, W. Xiao, V. Khadkikar, Dynamic modeling and control of interleaved flyback module-integrated converter for PV power applications, IEEE transactions on industrial electronics, 61(3) (2013) 1377-1388.
[16] S.Y. Chen, Small-signal model for a flyback converter with peak current mode control, IET Power Electronics, 7(4) (2014) 805-810.
[17] P.-J. Liu, H.-J. Chiu, Y.-K. Lo, Y.-J.E. Chen, A fast transient recovery module for dc–dc converters, IEEE Transactions on Industrial Electronics, 56(7) (2009) 2522-2529.

Uncorrected Proof

[18] Y.-C. Kang, C.-C. Chiu, M. Lin, C.-P. Yeh, J.-M. Lin, K.-H. Chen, Quasiresonant control with a dynamic frequency selector and constant current startup technique for 92% peak efficiency and 85% light-load efficiency flyback converter, IEEE transactions on power electronics, 29(9) (2013) 4959-4969.
[19] J. Font, L. Martinez, Modelling and analysis of a bidirectional boost converter with output filter, in: [1991 Proceedings] 6th Mediterranean Electrotechnical Conference, IEEE, 1991, pp. 1380-1383.
[20] H. El Fadil, F. Giri, Robust and nonlinear control of PWM DC-to-DC boost power converters, in: 2007 IEEE Power Electronics Specialists Conference, IEEE, 2007, pp. 407-412.
[21] F.A. Villarroel, J.R. Espinoza, M.A. Perez, R.O. Ramirez, C.R. Baier, D. Sbarbaro, J.J. Silva, M.A. Reyes, Stable shortest horizon FCS-MPC output voltage control in non-minimum phase boost-type converters based on input-state linearization, IEEE Transactions on Energy Conversion, 36(2) (2021) 1378-1391.
[22] W. Janke, Averaged models of pulse-modulated DC-DC power converters. Part I. Discussion of standard methods, Archives of Electrical Engineering, 61(4) (2012) 609-631.
[23] D.M. Sable, B.H. Cho, R.B. Ridley, Use of leading-edge modulation to transform boost and flyback converters into minimum-phase-zero systems, IEEE Transactions on Power Electronics, 6(4) (1991) 704-711.
[24] A. Goudarzian, A. Khosravi, H.A. Raeisi, Modeling, design and control of a modified flyback converter with ability of right-half-plane zero alleviation in continuous conduction mode, Engineering Science and Technology, an International Journal, 26 (2022) 101007.
[25] A. Goudarzian, A. Khosravi, H.A. Raeisi, Optimized sliding mode current controller for power converters with non-minimum phase nature, Journal of the Franklin Institute, 356(15) (2019) 8569-8594.
[26] B. Poorali, E. Adib, Right-half-plane zero elimination of boost converter using magnetic coupling with forward energy transfer, IEEE Transactions on Industrial Electronics, 66(11) (2019) 8454-8462.
[27] M.-F. Hung, K.-H. Tseng, Study on the corresponding relationship between dynamics system and system structural configurations—Develop a universal analysis method for eliminating the RHP-zeros of system, IEEE Transactions on Industrial Electronics, 65(7) (2017) 5774-5784.
[28] K. Kittipeerachon, C. Bunlaksananusorn, Feedback compensation design for switched mode power supplies with a right-half plane (RHP) zero, in: Second International Conference on Power Electronics, Machines and Drives (PEMD 2004). IET, 2004, pp. 236-241.
[29] A. Goudarzian, B. Mirzaeian Dehkordi, N. Abjadi, E. Adib, Design of a switched-capacitor boost converter utilizing magnetic coupling with capability of right-half plane zero elimination, IET Power Electronics, 14(1) (2021) 211-224.
[30] S. Ahmadzadeh, G. Arab Markadeh, N. Abjadi, Alleviating the right-half-plane zero effect on Z-source converter output voltage regulation using the cascaded sliding mode controller, IET Power Electronics, 13(15) (2020) 3419-3427.
[31] J.-W. Kim, J.-M. Choe, J.-S. Lai, Forward-flyback converter for LED driving with reduced number of components, in: 2017 IEEE Energy Conversion Congress and Exposition (ECCE), IEEE, 2017, pp. 3684-3687.
[32] H.-S. Lee, H.-J. Choe, S.-H. Ham, B. Kang, High-efficiency asymmetric forward-flyback converter for wide output power range, IEEE Transactions on Power Electronics, 32(1) (2016) 433-440.
[33] Y. Flicker, F.A. Himmelstoss, Combined isolated forward-flyback-converter with only one diode as battery charger, in: 2014 International Conference on Optimization of Electrical and Electronic Equipment (OPTIM), IEEE, 2014, pp. 512-518.
[34] M. Hua, B. Oian, A Hybrid Control Strategy for Forward flyback Converter with Improved Efficiency as an Interface to Low Voltage Renewable Sources, in: 2018 2nd IEEE Conference on Energy Internet and Energy System Integration (EI2), IEEE, 2018, pp. 1-5.
[35] P. Kuo, T. Liang, K. Tseng, J. Chen, S. Chen, An isolated high step-up forward/flyback active-clamp converter with output voltage lift, in: 2010 IEEE Energy Conversion Congress and Exposition, IEEE, 2010, pp. 542-548.
[36] M.S. Dall'Asta, V.B. Fuerback, T.B. Lazzarin, DCM Forward-Flyback converter integrated with a 5-order Cockcroft-Walton voltage multiplier: a steady-state and resonant current analysis, in: 2017 Brazilian Power Electronics Conference (COBEP), IEEE, 2017, pp. 1-6.
[37] S. Lee, Demystifying type II and type III compensators using op-amp and OTA for DC-DC converters, Texas Instruments Application Report SLVA662, July, (2014).